Derivation and utility of an Aβ-PET pathology accumulation index to estimate Aβ load

Antoine Leuzy, PhD,* Johan Lilja, PhD,* Christopher J. Buckley, PhD, Rik Ossenkoppele, PhD,
Sebastian Palmqvist, MD, PhD, Mark Battle, MSc, Gill Farrar, PhD, Dietmar R. Thal, MD, Shorena Janelidze, PhD,
Erik Stomrud, MD, PhD, Olof Strandberg, PhD, Ruben Smith, MD, PhD, and Oskar Hansson, MD, PhD

Correspondence
Dr. Leuzy
antoine.leuzy@med.lu.se

Abstract

Objective

To evaluate a novel β-amyloid (Aβ)-PET–based quantitative measure (Aβ accumulation index [Aβ index]), including the assessment of its ability to discriminate between participants based on Aβ status using visual read, CSF $Aβ_{42}/Aβ_{40}$, and post-mortem neuritic plaque burden as standards of truth.

Methods

One thousand one hundred twenty-one participants (with and without cognitive impairment) were scanned with Aβ-PET: Swedish BioFINDER, n = 392, [18F]flutemetamol; Alzheimer's Disease Neuroimaging Initiative (ADNI), n = 692, [18F]florbetapir; and a phase 3 end-of-life study, n = 100, [18F]flutemetamol. The relationships between Aβ index and standardized uptake values ratios (SUVR) from Aβ-PET were assessed. The diagnostic performances of Aβ index and SUVR were compared with visual reads, CSF $Aβ_{42}/Aβ_{40}$, and Aβ histopathology used as reference standards.

Results

Strong associations were observed between Aβ index and SUVR (R^2: BioFINDER 0.951, ADNI 0.943, end-of-life, 0.916). Both measures performed equally well in differentiating Aβ-positive from Aβ-negative participants, with areas under the curve (AUCs) of 0.979 to 0.991 to detect abnormal visual reads, AUCs of 0.961 to 0.966 to detect abnormal CSF $Aβ_{42}/Aβ_{40}$, and AUCs of 0.820 to 0.823 to detect abnormal Aβ histopathology. Both measures also showed a similar distribution across postmortem-based Aβ phases (based on anti-Aβ 4G8 antibodies). Compared to models using visual read alone, the addition of the Aβ index resulted in a significant increase in AUC and a decrease in Akaike information criterion to detect abnormal Aβ histopathology.

Conclusion

The proposed Aβ index showed a tight association to SUVR and carries an advantage over the latter in that it does not require the definition of regions of interest or the use of MRI. Aβ index may thus prove simpler to implement in clinical settings and may also facilitate the comparison of findings using different Aβ-PET tracers.

Classification of evidence

This study provides Class III evidence that the Aβ accumulation index accurately differentiates Aβ-positive from Aβ-negative participants compared to Aβ-PET visual reads, CSF $Aβ_{42}/Aβ_{40}$, and Aβ histopathology.

*These authors contributed equally to this work.

From the Clinical Memory Research Unit (A.L., J.L., R.O., S.P., S.J., E.S., O.S., R.S., O.H.), Department of Clinical Sciences, Lund University, Malmö; Department of Surgical Sciences, Nuclear Medicine and PET (J.L.), Uppsala University; Hermes Medical Solutions (J.L.), Stockholm, Sweden; GE Healthcare Life Sciences (C.J.B., M.B., G.F.), Amersham, UK; VU University Medical Center (R.O.), Neuroscience Campus Amsterdam, the Netherlands; Department of Neurology (S.P., R.S.) and Memory Clinic (E.S., O.H.), Skåne University Hospital, Lund, Sweden; Department of Imaging and Pathology (D.R.T.), Laboratory of Neuropathology, and Leuven Brain Institute (D.R.T.), Campus Gasthuisberg; and Department of Pathology (D.R.T.), UZ-Leuven, Belgium.

Go to Neurology.org/N for full disclosures. Funding information and disclosures deemed relevant by the authors, if any, are provided at the end of the article.

The Article Processing Charge was funded by the authors.

Glossary

Aβ = β-amyloid; **AD** = Alzheimer disease; **ADNI** = Alzheimer's Disease Neuroimaging Initiative; **AIC** = Akaike information criterion; **AUC** = area under the curve; **CERAD** = Consortium to Establish a Registry for Alzheimer's Disease; **CI** = cognitively impaired; **CU** = cognitively unimpaired; **DSM-IV** = *Diagnostic and Statistical Manual of Mental Disorders, 4th edition*; **ROI** = region of interest; **SUVR** = standardized uptake value ratio.

β-Amyloid (Aβ)-PET tracers such as $[^{18}F]$flutemetamol are currently approved for visual assessment only (whereby images are rated as negative/positive (normal/abnormal) by a trained rater).[1,2] Evidence suggests, however, that quantifying the amount of tracer retention in the brain may improve agreement between raters[3] and aid in the monitoring of treatment effects in anti-Aβ trials.[4] The most commonly used quantitative measure for Aβ-PET is the standardized uptake value ratio (SUVR), in which tracer concentration in cortical (target) regions is divided by that within a reference region assumed to be free of Aβ pathology. Although high-resolution structural MRI is ideally used to delineate these regions of interest (ROIs), this technique is not always available in clinical settings and is frequently contraindicated in elderly patients.[5]

In the absence of MRI, PET-only approaches can be used.[6] In this approach, a PET image is first transformed from a standardized coordinate space (spatial normalization), and ROIs are then defined with a probabilistic atlas. Using such an approach, we recently described a novel measure of brain Aβ burden (Aβ index).[7] Because it does not require the definition of ROIs, it is simpler to implement than SUVR. Here, we aimed (1) to compare Aβ index and SUVR in 3 independent cohorts; (2) to assess their ability to differentiate Aβ-positive and Aβ-negative participants using visual read, CSF Aβ$_{42}$/Aβ$_{40}$, or postmortem neuritic plaque burden as standards of truth; and (3) to assess whether a combination of visual read and Aβ index was superior to visual read alone to predict Aβ positivity using CSF Aβ$_{42}$/Aβ$_{40}$, and postmortem neuritic plaque burden as standards of truth. We hypothesized that across these aims, Aβ index would show noninferiority to SUVR.

Methods

Participants

Our population consisted of 1,121 participants with Aβ-PET from 3 separate cohorts: 392 from the Swedish BioFINDER study (clinical trial no. NCT01208675), scanned with $[^{18}F]$flutemetamol (251 cognitively unimpaired [CU], including 129 elderly controls, 122 with subjective cognitive decline, and 141 cognitively impaired [CI] participants with mild cognitive impairment), 629 from Alzheimer's Disease Neuroimaging Initiative (ADNI) (clinical trial no. NCT00106899) (246 CU controls and 383 CI participants [mild cognitive impairment]), scanned with $[^{18}F]$florbetapir, and 100 participants from a phase 3 end-of-life study (clinical

trial Nos. NCT01165554 and NCT02090855) who were scanned with $[^{18}F]$flutemetamol antemortem and autopsied after death.[8–10] Inclusion criteria for CU and CI individuals from BioFINDER and ADNI have been described elsewhere[11,12] and are described in the supplement (appendices e-1 and e-2, doi:10.5061/dryad.2547d7wnf). In the end-of-life study, participants were ≥55 years of age, terminally ill with a life expectancy <3 years, and with general health sufficient to allow completion of study procedures. Dementia, defined according to the DSM-IV criteria, was noted as present or absent, as reported in case notes. The relationship between Aβ index and SUVR was also examined in patients with Alzheimer disease (AD) dementia with CSF Aβ$_{42}$/Aβ$_{40}$ used as the standard of truth for Aβ status (BioFINDER, n = 25 with $[^{18}F]$flutemetamol PET available and n = 25 from ADNI with $[^{18}F]$florbetapir).

Standard protocol approvals, registrations, and patient consents

Written informed consent was obtained from all patients (or guardians of patients) participating in the study (consent for research). Ethics approval for BioFINDER was given by the Regional Ethical Committee of Lund University. Approval for PET imaging was obtained from the Swedish Medical Products Agency and the local Radiation Safety Committee at Skåne University Hospital. For the ADNI and end-of-life cohorts, study protocols were approved by local ethical committees.

Image acquisition and processing

For BioFINDER, $[^{18}F]$flutemetamol studies were performed with a Philips Gemini TF PET/CT scanner (Philips Medical Systems, Amsterdam, the Netherlands) over the interval of 90 to 110 minutes after injection; data were acquired in list mode and binned into frames with an iterative Vue Point HD algorithm (6 subsets, 18 iterations with 3-mm filter and no time-of-flight correction). All participants underwent 3T MRI scans (Siemens MAGNETOM Prisma, Munich, Germany), acquiring isometric 1-mm^3 T1-weighted magnetization-prepared rapid gradient echo images. For ADNI, $[^{18}F]$florbetapir image data acquired 50 to 70 minutes after injection[13] and T1-weighted MRI scans using a sagittal volumetric magnetization-prepared rapid gradient echo sequence acquired at 3T were used.[14] For the phase 3 end-of-life study, $[^{18}F]$flutemetamol PET images were acquired on PET/CT cameras over the interval of 90 to 110 minutes after injection. Because both ADNI and the phase 3 end-of-life study were multicentric in nature, images were smoothed to achieve a uniform imaging resolution.

Aβ-PET images were spatially normalized with 2 approaches: an MRI-driven approach included in SPM12 and a PET-driven principal component approach.[7] For the end-of-life cohort, normalization of [18F]flutemetamol images was performed only with the principal component approach because MRI was not available. The purpose of this dual approach was to ensure that SUVRs from the principal component approach were highly correlated with those derived with the MRI-driven gold standard approach. The complete details of the principal component approach can be found in the original publication.[7] Briefly, tracer-specific principal component images are first calculated by singular value decomposition of Aβ-PET SUVR images. Two principal components were chosen because they captured ≈95% of the variance in the dataset. The first principal component represents the average of all the images the dataset; the second, the different between Aβ-positive and Aβ-negative images (i.e., specific binding). A synthetic template ($I_{Synthetic}$) can then be modeled as a linear combination of the first and second principal component images (I_{PC1} and I_{PC2}, respectively). As part of this operation, I_{PC2} is multiplied by a weighting factor (Aβ index; i.e., $I_{Synthetic} = I_{PC1} + $ Aβ index $\times I_{PC2}$) representing a global measure of brain Aβ pathology. Here, a positive Aβ index yields a template with a more Aβ-positive appearance and a negative value yields a template with a more Aβ-negative appearance. With the use of an algorithm that incorporates both the Aβ index and the parameters required for the spatial transformation, the synthetic template can then be used to normalize Aβ-PET images.

In the present study, preexisting synthetic templates derived from phase 2 studies were used for [18F]flutemetamol[15] and [18F]florbetapir.[16,17] After spatial normalization of [18F]flutemetamol and [18F]florbetapir scans, 2 sets of SUVRs were calculated (one for each normalization method) for BioFINDER and ADNI participants using a composite cortical ROI—encompassing brain regions typically showing high Aβ load in AD, including frontal, temporal, and parietal cortices, precuneus, anterior striatum, and insular cortex—and the pons and cerebellum as reference tissues[18] for [18F]flutemetamol and [18F]florbetapir, respectively. As described, SUVR values for [18F]flutemetamol scans from the end-of-life cohort were based on the principal component–based normalization alone.

The term principal component herein refers to the principal component–driven normalization approach (and, for instance, SUVR values derived from images normalized using this approach), not the Aβ index per se (which is generated when the principal component–driven approach is used for spatial normalization).

CSF biomarkers

Lumbar puncture and CSF handling followed structured protocols in the BioFINDER and ADNI studies.[11] In BioFINDER, the fully automated Elecsys assays (Roche Diagnostics, Indianapolis, IN) were used, as described elsewhere,[19,20] with samples analyzed at the Clinical Neurochemistry Laboratory, University of Gothenburg, Sweden. In ADNI, CSF $A\beta_{42}/A\beta_{40}$ was determined from $A\beta_{42}$ and $A\beta_{40}$ measurements derived from a liquid chromatography with tandem mass spectrometric detection (ultraperformance liquid chromatography–mass spectrometry) method,[21] with samples analyzed in the Biomarker Research Laboratory, University of Pennsylvania.

Postmortem Aβ pathology assessment

Postmortem-based estimates of Aβ plaque pathology were based on autopsy brain tissue previously collected in support of the GE067-007/GE-067-026 phase 3 clinical trials for [18F] flutemetamol PET.[22] As described elsewhere,[10] after formalin fixation, brains were coronally sliced and macroscopically screened. The Bielschowsky silver method was then applied to paraffin-embedded tissue from 8 neocortical regions, as defined by the Consortium to Establish a Registry for Alzheimer's Disease (CERAD).[23] In each region, neuritic plaque densities were recorded as 0 (no plaques), 1 (sparse; 1–5 plaques), 2 (moderate; 6–19 plaques), or 3 (frequent; >20 plaques), per 100× field of view.[23,24] A modified CERAD-based assessment approach was then applied whereby the arithmetic mean of neuritic plaque density was calculated across the 8 investigated regions (30 measures per region), giving a continuous variable. Aβ phases 9 describing the hierarchical spreading of Aβ plaque pathology in the brain were determined after screening the Aβ-stained sections (anti-Aβ 4G8 antibodies) for plaque distribution.[9]

Definition of Aβ status

Aβ status (positive/negative), as a standard of truth, was defined with 3 approaches: in ADNI and BioFINDER using consensus read of Aβ-PET uptake images and CSF $A\beta_{42}/A\beta_{40}$, and in the end-of-life trial using the postmortem–based Bielschowsky histopathology score. For CSF $A\beta_{42}/A\beta_{40}$, cutoffs of 0.059 (BioFINDER)[25] and 0.137 (ADNI) were used, based on gaussian mixture modeling applied to the BioFINDER and ADNI cohorts. For Bielschowsky silver stain, each assessed brain region was scored from 0 to 3 (calculated as the arithmetic mean of 30 measures); a score >1.5, previously shown to represent the threshold between the categories of sparse and moderate neuritic plaques,[10] in any of the 8 investigated regions was considered abnormal, with the brain classified as Aβ positive.

Statistical analyses

Between-group characteristics were compared with the Kruskal-Wallis or Fisher exact test. The relationship between Aβ index and SUVR from [18F]flutemetamol and [18F]florbetapir was examined with linear regression and coefficient of determination (R^2). Receiver operating characteristic analyses were performed to generate area under the curve (AUC) values for both Aβ index and SUVR. Differences in AUC values for these measures were evaluated with bootstrap (n = 1,000) procedures. To assess the added clinical value of the Aβ index, AUC and Akaike information criterion (AIC) values from binary logistic regression models (using CSF $A\beta_{42}/A\beta_{40}$ [BioFINDER and ADNI] and Bielschowsky histopathology

Table 1 BioFINDER and ADNI cohort characteristics

Characteristic	BioFINDER		ADNI	
	CU	CI	CU	CI
No.	251	141	246	383
Age, mean (SD) [range], y	71.92 (5.15) [59, 85]	70.91 (5.58) [60, 80]	72.16 (5.79) [56, 89]	71.05 (7.53) [55, 89]
Male/female, n (% male)	109/142 (43)	88/53 (62)	121/125 (49)	208/175 (54)
Education, y	12.17 (3.39)	11.14 (3.29)	16.82 (2.49)	16.3 (2.59)
MMSE score	28.79 (1.23)	27.26 (1.71)	29.05 (1.18)	28.11 (1.73)
$APOE$ ε4+, n (%)	91 (36)	66 (47)	51 (28)	221 (58)
CSF $A\beta_{42}/A\beta_{40}$+, n (%)	71 (28)	88 (62)	71 (29)	211 (55)
Aβ PET, visual read+, n (%)	48 (19)	79 (56)	51 (21)	185 (48)
Aβ PET, SUVR	0.65 (0.15)	0.81 (0.21)	1.17 (0.19)	1.28 (0.24)
Aβ PET, Aβ index	−0.79 (0.63)	−0.21 (0.78)	−0.82 (0.84)	−0.23 (0.95)

Abbreviations: Aβ = β-amyloid; CI = cognitively impaired; CU = cognitively unimpaired; MMSE = Mini-Mental State Examination; SUVR = standardized uptake values ratio.

[end-of-life cohort] as the outcome variables [positive/negative]) and visual read (model 1) or visual read in combination with Aβ index (continuous, model 2) were compared. For comparison, a third model combining visual read and SUVR was included. All analyses were performed in R (version 3.5.3; R-project.org/), with significance set at $p < 0.05$, 2 sided.

Primary research question

The primary research question was how Aβ index and SUVR from Aβ PET compare in their ability to differentiate participants according to their Aβ status. This study provides Class III evidence that the Aβ accumulation index accurately differentiates Aβ-positive from Aβ-negative participants compared to Aβ-PET visual reads, CSF $A\beta_{42}/A\beta_4$, and Aβ histopathology.

Data availability

Anonymized study data for the primary analyses presented in this report are available on request from any qualified investigator for purposes of replicating the results.

Table 2 End-of-life cohort characteristics

Characteristic	Dementia	No dementia	All participants
No.	85	15	100
Age, mean (SD) [range], y	82.71 (7.91) [60, 96]	78.40 (11.09) [60, 93]	82.10 (8.54) [60, 96]
Male/female, n (% male)	32/53 (38)	5/10 (33)	42/58 (58)
Dementia, n (%)	85 (100)	0 (0)	85 (85)
Bielschowsky silver stain	2.00 (0.79)	1.31 (1.13)	1.90 (0.88)
Thal Aβ phase 1/2/3/4/5, n	6/4/10/21/44	5/1/4/2/3	11/5/14/24/46
Braak tau stage, I–II/III–IV/V–VI, n	14/17/50	4/8/1	18/25/51
CERAD, N/S/M/F, n	4/18/26/37	5/1/6/2	9/20/32/39
Aβ PET, visual read+, n (%)	67 (79)	5/10 (33)	72 (72)
Aβ PET, SUVR	0.88 (0.20)	0.79 (0.22)	0.87 (0.21)
Aβ PET, Aβ index	0.31 (0.81)	−0.19 (0.89)	0.23 (0.84)
Scan-to-death time interval, d	234.95 (215.48)	234.13 (189.26)	234.83 (210.86)

Abbreviations: Aβ = β-amyloid; CERAD = Consortium to Establish a Registry for Alzheimer's Disease; N/S/M/F = none/sparse/moderate/frequent; SUVR = standardized uptake values ratio.

Results

Cohort characteristics are summarized in table 1 (BioFINDER and ADNI) and table 2 (end-of-life study). Among the 85 cases in the end-of-life cohort with an antemortem diagnosis of dementia, 28 (33%) had a postmortem neuropathologic diagnosis of pure AD, 33 (39%) had a diagnosis of AD plus at least 1 other pathology (e.g., cerebral amyloid angiopathy or TAR DNA-binding protein 43), and 24 (28%) had a non-AD pathology such as Lewy body or vascular dementia. Figure 1 provides an overview of the steps required to generate the Aβ index. Principal component images for [18F]flutemetamol and [18F]florbetapir are provided in figure e-1 (doi:10.5061/dryad.2547d7wnf). Comparison of SUVR values using principal component– and MRI-(SPM12) driven normalization approaches showed good agreement (figure e-2), with R^2 values of 0.997 for [18F]flutemetamol and 0.995 for [18F]florbetapir ($p < 0.001$). Characteristics of AD dementia participants are summarized in table e-1.

Strong associations were observed between Aβ index– and principal component–derived SUVR values in both cohorts (BioFINDER R^2 = 0.951 [95% confidence interval 0.933–0.961], ADNI R^2 = 0.943 [95% confidence interval 0.927–0.952], $p < 0.001$) (figure 2). Comparison of receiver operating characteristic curve–derived AUC values from Aβ index and SUVR showed that both measures performed equally well in differentiating Aβ-positive from Aβ-negative participants, with both visual read (AUCs 0.979 [95% confidence interval 0.972–0.989] to 0.991 [95% confidence interval 0.972–0.989]) and CSF Aβ$_{42}$/Aβ$_{40}$ (AUCs 0.961 [95% confidence interval 0.939–0.983] to 0.971 [95% confidence interval 0.949–0.981]) used as standards of truth (figure 3), with no significant difference found between AUC values. Similar findings were obtained for AD dementia cases (figure e-3; doi:10.5061/dryad.2547d7wnf).

In the [18F]flutemetamol end-of-life cohort, we found that both Aβ index and SUVR could predict abnormal Bielschowsky silver stain scores (AUCs 0.820 [95% confidence interval 0.716–0.923] to 0.823 [95% confidence interval 0.725–0.921]) and visual read outcomes (AUCs 0.938 [95% confidence interval 0.889–0.984] to 0.949 [95% confidence interval, 0.911–0.988]) (figure 4), with no significant difference found between AUC values. With the Aβ phases (Thal et al.[26]) as neuropathologic readout, a similar distribution was seen for [18F]flutemetamol Aβ index and SUVR across Aβ phases (figure 4). Comparison of SUVR and Aβ index measures between Aβ phases (i.e., phase 1 vs 2, 2 vs 3, 3 vs 4, and 4 vs 5) showed significant differences for both measures between phases for the contrasts phase 3 vs 4 (SUVR and Aβ index, $p < 0.001$) and phase 4 vs 5 (SUVR and Aβ index, $p < 0.01$).
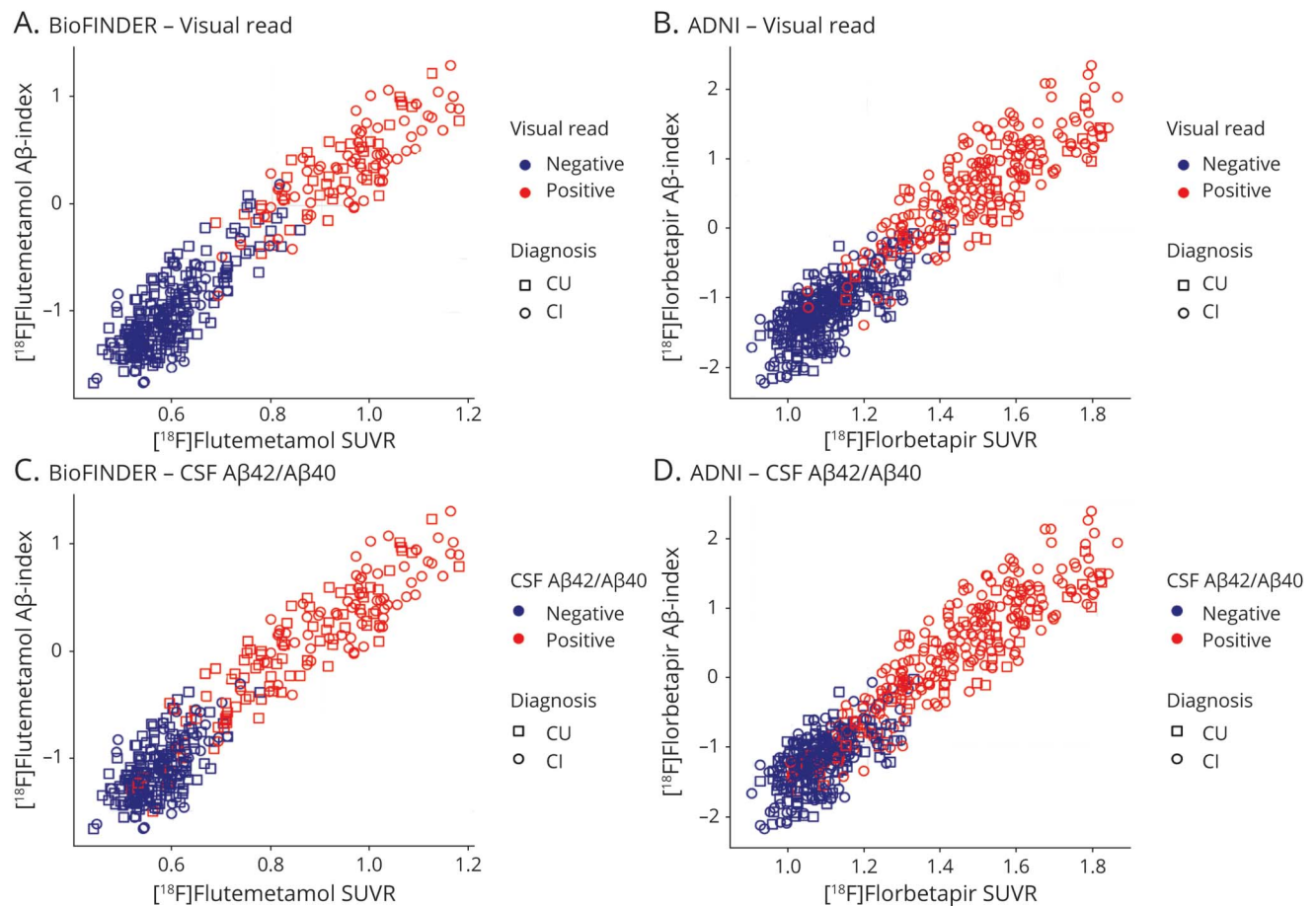
Finally, we studied whether a combination of Aβ index and visual read was superior to visual read alone. Compared to the binary logistic regression model using only visual read as a predictor, the addition of the Aβ index resulted in a significant increase in AUC (Aβ status as outcome) using CSF Aβ$_{42}$/Aβ$_{40}$ (BioFINDER 0.868 [95% confidence interval 0.843 to 0.894 vs 0.962 [95% confidence interval 0.932–0.987], $p < 0.001$; ADNI 0.881 [95% confidence interval 0.856–0.906] vs 0.943 [95% confidence interval 0.923–0.962], $p < 0.001$) and Bielschowsky histopathology (0.910 [95% confidence interval

Figure 1 Flow diagram providing an overview of the MRI-free normalization method
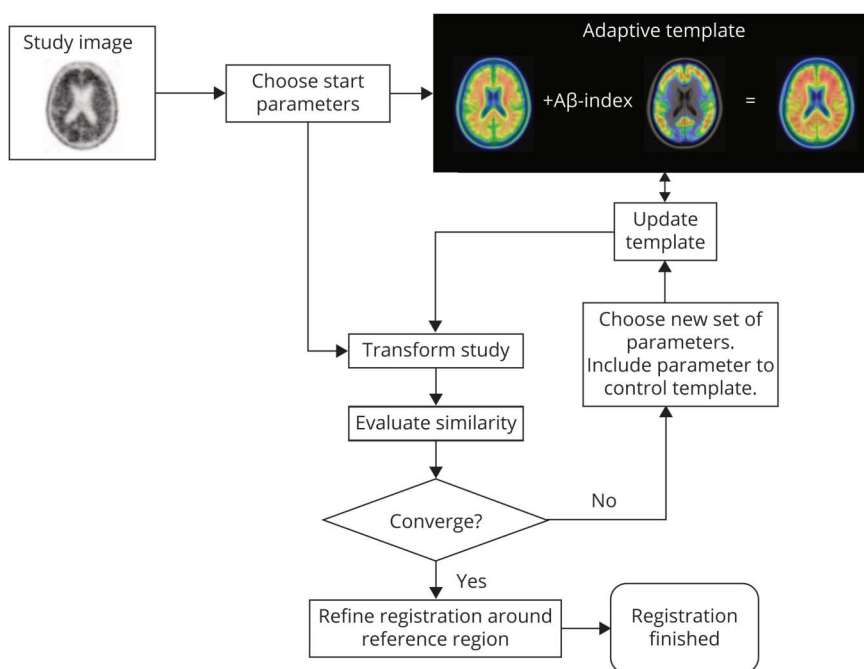
Shown are the steps required to generate the adaptive template and to spatially normalize the input β-amyloid (Aβ)-PET image. In the upper right corner, the role of the Aβ index is illustrated: the first principal component image is combined with a weighted version of the second component image, yielding a template image optimal for the input image.

Figure 2 Scatterplots showing the relationship between Aβ index and SUVR

A. BioFINDER – Visual read
B. ADNI – Visual read
C. BioFINDER – CSF Aβ42/Aβ40
D. ADNI – CSF Aβ42/Aβ40

The association between β-amyloid (Aβ) index and standardized uptake values ratio (SUVR) is shown for [^{18}F]flutemetamol (BioFINDER cohort; A and C) and [^{18}F]florbetapir (Alzheimer's Disease Neuroimaging Initiative [ADNI] cohort; B and D) PET, with Aβ status defined using (A and B) visual read and (C and D) CSF Aβ$_{42}$/Aβ$_{40}$ as standards of truth for Aβ status. CI = cognitively impaired; CU = cognitively unimpaired.

0.883 to 0.937] vs 0.961 [95% confidence interval 0.936–0.986], $p < 0.05$). Moreover, addition of the Aβ index resulted in an improved model fit (AIC) (using CSF Aβ$_{42}$/Aβ$_{40}$: BioFINDER 253.94 vs 167.78, ADNI 400.59 vs 328.89; using Bielschowsky histopathology in the end-of-life cohort: 60.24 vs 53.86).[27] Similar findings were observed when SUVR was used for both AUC (AUC: CSF Aβ$_{42}$/Aβ$_{40}$, BioFINDER 0.868 [95% confidence interval 0.843–0.894] vs 0.942 [95% confidence interval 0.914–0.968], $p < 0.001$; ADNI 0.881 [95% confidence interval 0.859–0.905] vs 0.954 [95% confidence interval 0.925–0.983], $p < 0.001$; Bielschowsky, end-of-life cohort 0.910 [95% confidence interval 0.889–0.933] vs 0.942 [95% confidence interval 0.917–0.969], $p < 0.05$) and AIC (CSF Aβ$_{42}$/Aβ$_{40}$, BioFINDER 253.94 vs 161.08; ADNI 400.59 vs 306.31; and in the end-of-life cohort using Bielschowsky histopathology: 60.24 vs 56.94).

Discussion

The objective of the present study was to assess the relationship between Aβ index and Aβ-PET SUVR, including a comparison of the ability of both measures to differentiate between participants on the basis of their Aβ status, using several standards of truth (visual read, CSF Aβ$_{42}$/Aβ$_{40}$, and postmortem Aβ histopathology). First, using both [^{18}F]flutemetamol and [^{18}F]florbetapir, we showed that the principal component–based approach to normalization was precise and accurate, with SUVRs from this approach correlating highly with those derived from the MRI-based method in SPM. Using this PET-driven approach, we then showed a close correspondence between the Aβ index and SUVR, with both measures performing equally well in identifying Aβ-positive cases and showing a similar pattern of increase across postmortem Aβ phases. Finally, we showed that the addition of the Aβ index improved prediction of Aβ status relative to the use of visual read alone.

Given recent evidence showing that Aβ-PET imaging led to changes in the clinical management of CI individuals,[28] the importance of accurate and reproducible Aβ image interpretation is clear. Although the visual assessment of Aβ scans as positive or negative has been shown to be an

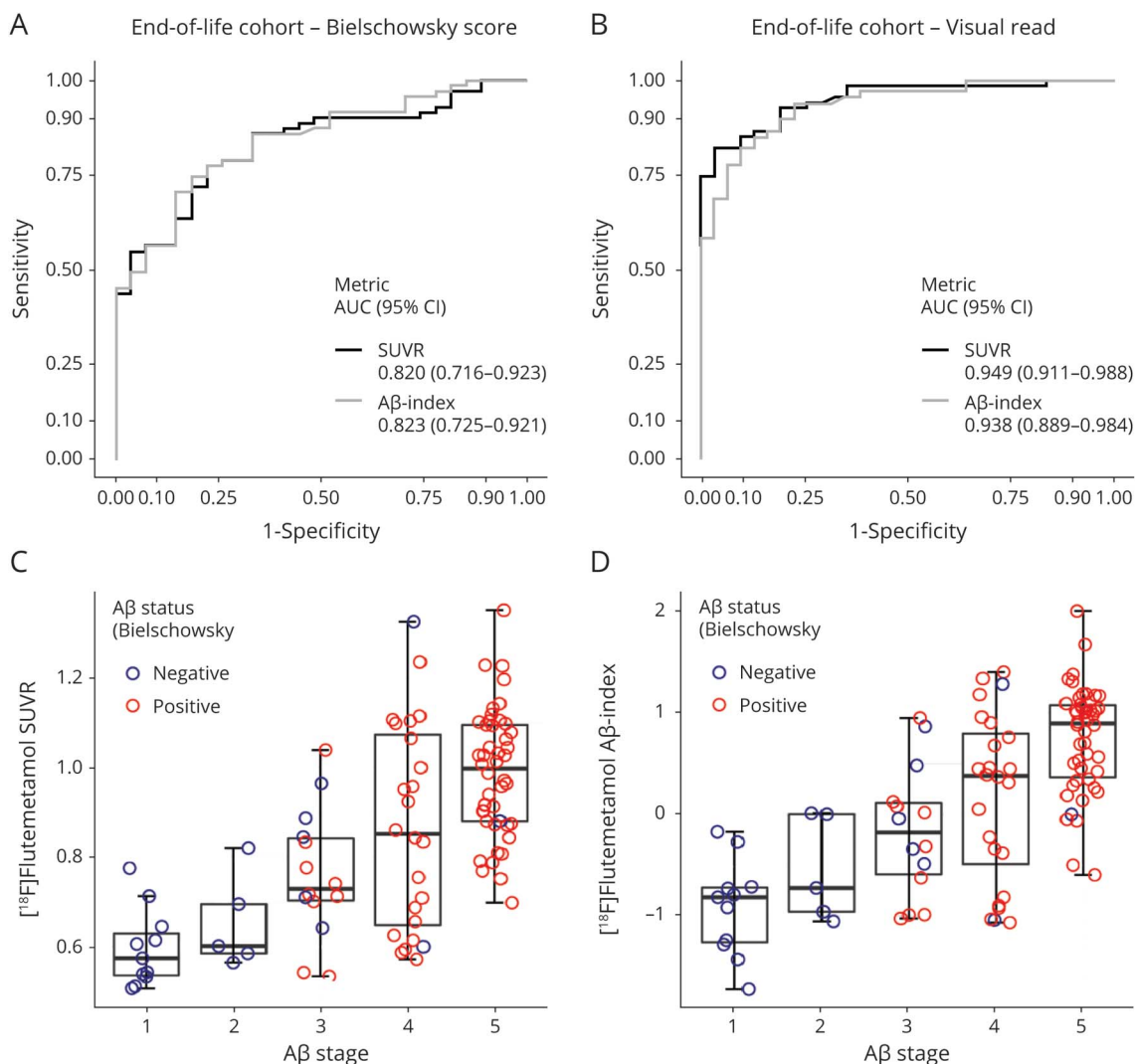**Figure 3** Receiver operating characteristic plots using Aβ index and SUVR
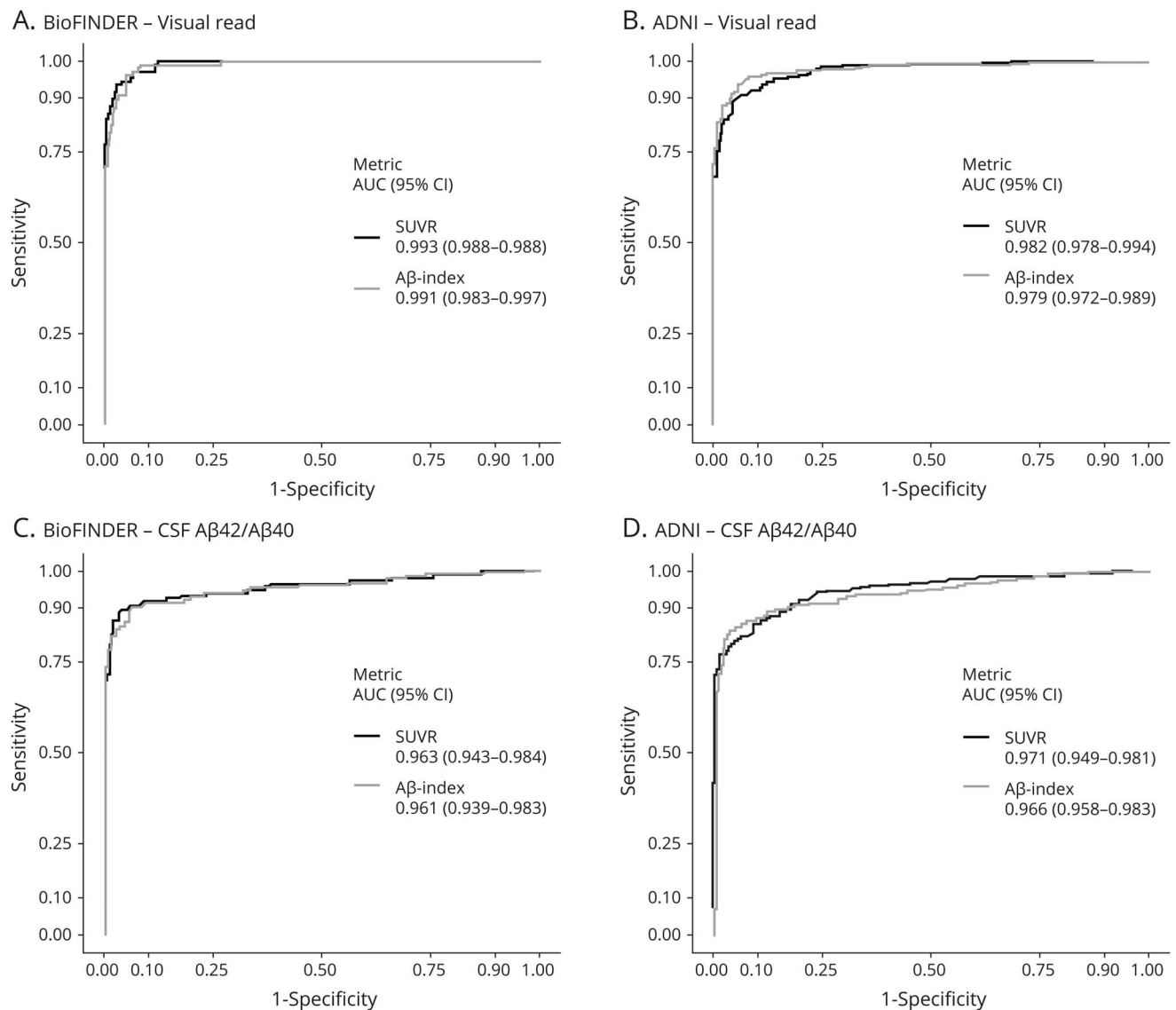
Receiver operating characteristic plots for [^{18}F]flutemetamol (BioFINDER cohort; A and C) and [^{18}F]florbetapir (Alzheimer's Disease Neuroimaging Initiative [ADNI cohort]; B and D) for distinguishing β-amyloid (Aβ)–negative and Aβ-positive participants using (A and B) visual read and (C and D) CSF Aβ$_{42}$/Aβ$_{40}$ as standards of truth for Aβ status. CI = confidence interval; SUVR = standardized uptake values ratio.

adequately sensitive method with respect to postmortem estimates of plaque burden, studies have shown significant variability across readers.[29,30] Findings from several studies indicate that use of quantification could prove a helpful adjunct to visual interpretation,[31–34] similar to other areas of nuclear medicine involving PET imaging.[35,36] Quantification of Aβ-PET images using SUVR derived from commercial software packages, for instance, has been shown to improve the accuracy of visual reads in clinically relevant cases.[37] This was also the case in the present study, in which the addition of the Aβ index improved prediction of histopathology based Aβ status. The addition of an objective measure such as Aβ index or SUVR will probably be even more important in clinical practice, where many readers are not as experienced as those evaluating clinical PET images in academic research

studies or clinical trials. The Aβ index, along with a cutoff indicating whether the scan is positive, could easily be incorporated into currently available commercial software.[38] Quantification has also been shown to result in more consistent detection of early Aβ plaque pathology in CU older adults.[39] This finding in particular is of importance given that CU older individuals who are accumulating Aβ in the Aβ-negative range, where visual read alone is likely to prove insensitive, may prove a key target population for anti-Aβ clinical trials.[40]

A fundamental step prerequisite to quantification in PET is the spatial transformation of data into a common space (i.e., spatial normalization). SUVR values derived with the proposed principal component method were tightly

Figure 4 Findings from the [^{18}F]flutemetamol phase 3 end-of-life cohort

Receiver operating characteristic plots (A–D) for distinguishing β-amyloid (Aβ)–negative and Aβ-positive participants using the Bielschowsky silver stain score and visual read are shown in panels A and B, respectively. CI = confidence interval; SUVR = standardized uptake values ratio.

correlated to those based on the dual-scan (MRI, PET) MRI-driven approach used in SPM, indicating that accurate spatial normalization was achieved. Furthermore, this method removes the need for a separate MRI scan; this is a highly desirable quality given that MRI is not always available as part of routine clinical workup and can be complicated by high rates of nonparticipation due to difficulty lying still during the examination, claustrophobia, contraindications such as pacemakers or metallic implants, and other reasons.[5] In addition, removing the need for MRI would decrease the burden placed on patients and caregivers, and a short CT scan is often adequate to exclude secondary causes of cognitive impairment such as subdural hematoma and tumors and can be done in conjunction with the PET scan. In terms of clinical translation, additional studies are required to address whether the improvements in interreader agreement seen when SUVR is added to visual read of Aβ-PET images[3,37] are also observed when the Aβ index is used.

In both BioFINDER and ADNI, a range of Aβ index values were observed for a given SUVR level. Despite identical SUVR levels, interpreted as indicating no difference in overall brain Aβ load, differences in the topography of Aβ pathology can be seen between participants. These interparticipant differences may explain the variability seen in Aβ index for a given SUVR value. Although Aβ index as a global metric of Aβ pathology may be of greatest interest from a clinical standpoint, further work addressing whether Aβ index can in fact also provide information about Aβ pathology within different brain regions may be of interest, particularly with respect to the validation of PET-based Aβ staging schemes[26,41] and with an eye to testing this approach with tau PET. However, the finding that Aβ index values were only significantly different between advanced Aβ phases (3 vs 4 and 4 vs 5), as for SUVR, is in line with earlier work showing that [^{18}F]flutemetamol PET detects Aβ pathology primarily in cases with advanced plaque pathology (i.e., Aβ phase ≥4).[42]

Two previous studies have used adaptive[43] and principal component–derived templates[44] with Aβ-PET. In the first study[43] using [18F]flutemetamol PET, intercept and slope images were generated using linear regression; the slope image in combination with a weight is then used to generate a template. While the slope image is similar to our second principal component image, the principal component–derived template appeared to provide greater accuracy.[7] In the second study[44] an adaptive template was generated with [11C]-Pittsburgh compound B and spline-based transformations for the normalization step; due to the use of splines, however, the computational time of their approach exceeds 6 hours, in contrast to an average processing time of ≈20 seconds per participant with our method. Furthermore, a novel measure called Aβ load ($A\beta_L$) was recently presented.[24] A metric of global Aβ burden, $A\beta_L$ is calculated as a linear combination of 2 canonical images (nonspecific binding and a carrying capacity image representing the maximum possible concentration of Aβ).[45] Although these images and $A\beta_L$ are conceptually similar to our principal component images and Aβ index, respectively, in contrast to the AβL method[45] our method does not require the use of MRI and is several orders of magnitude faster from a per-participant computational standpoint.

Due to variability in the acquisition windows used for scanning, analysis methods, and ROI selection, quantitatively expressed Aβ-PET outcome data cannot currently be directly compared. In an attempt to address this, a method was proposed whereby Aβ-PET values are standardized to a 100-point scale using a linear scaling procedure. The units of this scale are called Centiloids, with 0 representing the average uptake in Aβ-negative participants and 100 representing the average in patients with mild to moderate AD.[18] While the Aβ index could be converted to Centiloids via the prescribed steps, the fact that it is independent of ROI definition suggests that it could be directly comparable between Aβ-PET tracers, without the need for conversion to the Centiloid scale. This would require, however, that a universal adaptive template be established by applying a principal component–based analysis to a dataset comprising existing commercial Aβ-PET tracers. Future work is required to explore this possibility.

Strengths of the present study include the use of 2 different Aβ-PET tracers across 3 independent cohorts, a large sample size, and the use of multiple standards of truth for defining Aβ-status. Certain limitations apply as well, however. First, cases of AD dementia or non-AD neurodegenerative disorders were not included. The close association of Aβ index to SUVR across a range of values, however, indicates that the relationship between these metrics is governed by brain Aβ levels and is therefore independent of clinical diagnosis. Therefore, omitting these diagnostic groups is unlikely to have affected our results. Second, the patients in the Swedish BioFINDER study have been recruited in a consecutive fashion at 3 different memory clinics, with ≈90% of these referred by primary care physicians. In the ADNI study, the patients were recruited from many different clinics and thereby represent a more selected sample. Still, the results obtained for the Aβ-PET pathology accumulation index in both these studies are very similar. In light of findings showing that clinic-based cohorts such as ADNI and, to a lesser extent, BioFINDER might have a lower prevalence of infarcts and mixed pathologies,[46] further studies are required to validate the use of Aβ index in community-based cohorts. Third, we did not examine the effect of atrophy on Aβ and SUVR. Because neurodegenerative disorders such as AD are accompanied by progressive cortical atrophy, susceptibility to partial volume effects increases, which, in the case of Aβ-PET, can diminish estimates of tracer retention. While partial volume effects were likely present to some degree in the BioFINDER and ADNI cohorts, the strong correlation between Aβ index and SUVR across participants suggests that these metrics were not differentially affected. We cannot exclude, however, that the strength of the association between Aβ index and SUVR may be affected by atrophy in individual cases. Although fully quantitative measures (i.e., binding potential or distribution volume ratio) would have been preferable over the use of SUVR—due the sensitivity of SUVR to cerebral blood flow–induced changes in tracer kinetics[47]—binding potential and distribution volume ratio require the use of dynamic data, which were not available. Lastly, in addition to the lack of antemortem diagnosis (beyond the presence or absence of dementia), there was considerable variation in the PET to postmortem delay (scan-to-death time interval) in the end-of-life cohort; although this may have resulted in changes in Aβ burden not captured by the initial [18F]flutemetamol studies, our findings with the Aβ phases and prior work showing that the PET-to-death time interval did not affect the diagnostic performance of [18F]flutemetamol[48] argue against this being the case.

Although the proposed Aβ index showed a tight association to SUVR values and similar discriminative and predictive performance, it carries an advantage over SUVR in that it does not require the definition of target and reference regions. The Aβ index may therefore prove simpler to implement in clinical settings. Further work is needed to address whether the Aβ index could be implemented as a common measure across different Aβ tracers and analytical approaches, without the need for standardization to the Centiloid scale. An Aβ index–driven approach would require the availability of a hybrid template derived from all 3 commercially available Aβ tracers. This template is under development and will be the focus of future work.

Study funding

Disclosure

Publication history

Appendix Authors

Name	Location	Contribution
Antoine Leuzy, PhD	Lund University, Malmö, Sweden	Design and conceptualized study; analyzed the data; performed the statistical analyses; drafted the manuscript for intellectual content
Johan Lilja, PhD	Lund University, Malmö, Sweden	Design and conceptualized study; analyzed the data; drafted the manuscript for intellectual content
Christopher J. Buckley, PhD	GE Healthcare Life Sciences, Amersham, UK	Design and conceptualized study; analyzed the data; drafted the manuscript for intellectual content
Rik Ossenkoppele, PhD	Lund University, Malmö, Sweden; VU University Medical Center, Amsterdam, the Netherlands	Major role in the acquisition of data; interpreted the data; revised the manuscript for intellectual content
Sebastian Palmqvist, MD, PhD	Lund University, Malmö, Sweden; Skåne University Hospital, Lund, Sweden	Major role in the acquisition of data; interpreted the data; revised the manuscript for intellectual content
Mark Battle, MSc	GE Healthcare Life Sciences, Amersham, UK	Major role in the acquisition of data; interpreted the data; revised the manuscript for intellectual content
Gill Farrar, PhD	GE Healthcare Life Sciences, Amersham, UK	Major role in the acquisition of data; interpreted the data; revised the manuscript for intellectual content

Appendix *(continued)*

Name	Location	Contribution
Dietmar R. Thal, MD	Leuven Brain Institute, Leuven, Belgium; UZ-Leuven, Leuven, Belgium	Design and conceptualized study; analyzed the data; drafted the manuscript for intellectual content
Shorena Janelidze, PhD	Lund University, Malmö, Sweden	Major role in the acquisition of data; interpreted the data; revised the manuscript for intellectual content
Erik Stomrud, MD, PhD	Lund University, Malmö, Sweden; Skåne University Hospital, Lund, Sweden	Major role in the acquisition of data; interpreted the data; revised the manuscript for intellectual content
Olof Strandberg, PhD	Lund University, Malmö, Sweden	Major role in the acquisition of data; interpreted the data; revised the manuscript for intellectual content
Ruben Smith, MD, PhD	Lund University, Malmö, Sweden; Skåne University Hospital, Lund, Sweden	Major role in the acquisition of data; interpreted the data; revised the manuscript for intellectual content
Oskar Hansson, MD, PhD	Lund University, Malmö, Sweden; Skåne University Hospital, Lund, Sweden	Design and conceptualized study; analyzed the data; drafted the manuscript for intellectual content

References

1. Seibyl J, Catafau AM, Barthel H, et al. Impact of training method on the robustness of the visual assessment of 18F-florbetaben PET scans: results from a phase-3 study. J Nucl Med 2016;57:900–906.
2. Buckley CJ, Sherwin PF, Smith AP, Wolber J, Weick SM, Brooks DJ. Validation of an electronic image reader training programme for interpretation of [18F]flutemetamol beta-amyloid PET brain images. Nucl Med Commun 2017;38:234–241.
3. Nayate AP, Dubroff JG, Schmitt JE, et al. Use of standardized uptake value ratios decreases interreader variability of [18F] florbetapir PET brain scan interpretation. AJNR Am J Neuroradiol 2015;36:1237–1244.
4. Schmidt ME, Chiao P, Klein G, et al. The influence of biological and technical factors on quantitative analysis of amyloid PET: points to consider and recommendations for controlling variability in longitudinal data. Alzheimers Dement 2015;11:1050–1068.
5. Tell GS, Lefkowitz DS, Diehr P, Elster AD. Relationship between balance and abnormalities in cerebral magnetic resonance imaging in older adults. Arch Neurol 1998;55:73–79.
6. Desikan RS, Segonne F, Fischl B, et al. An automated labeling system for subdividing the human cerebral cortex on MRI scans into gyral based regions of interest. Neuroimage 2006;31:968–980.
7. Lilja J, Leuzy A, Chiotis K, Savitcheva I, Sorensen J, Nordberg A. Spatial normalization of [(18)F]flutemetamol PET images utilizing an adaptive principal components template. J Nucl Med 2019;60:285–291.
8. Beach TG, Thal DR, Zanette M, Smith A, Buckley C. Detection of striatal amyloid plaques with [18F]flutemetamol: validation with postmortem histopathology. J Alzheimers Dis 2016;52:863–873.
9. Thal DR, Beach TG, Zanette M, et al. Estimation of amyloid distribution by [(18)F]flutemetamol PET predicts the neuropathological phase of amyloid beta-protein deposition. Acta Neuropathol 2018;136:557–567.
10. Ikonomovic MD, Buckley CJ, Heurling K, et al. Post-mortem histopathology underlying beta-amyloid PET imaging following flutemetamol F 18 injection. Acta Neuropathol Commun 2016;4:130.
11. Palmqvist S, Zetterberg H, Blennow K, et al. Accuracy of brain amyloid detection in clinical practice using cerebrospinal fluid beta-amyloid 42: a cross-validation study against amyloid positron emission tomography. JAMA Neurol 2014;71:1282–1289.
12. Petersen RC, Aisen PS, Beckett LA, et al. Alzheimer's Disease Neuroimaging Initiative (ADNI): clinical characterization. Neurology 2010;74:201–209.
13. Landau SM, Mintun MA, Joshi AD, et al. Amyloid deposition, hypometabolism, and longitudinal cognitive decline. Ann Neurol 2012;72:578–586.
14. Jack CR Jr, Bernstein MA, Fox NC, et al. The Alzheimer's Disease Neuroimaging Initiative (ADNI): MRI methods. J Magn Reson Imaging 2008;27:685–691.

15. Vandenberghe R, Van Laere K, Ivanoiu A, et al. 18F-flutemetamol amyloid imaging in Alzheimer disease and mild cognitive impairment: a phase 2 trial. Ann Neurol 2010; 68:319–329.

16. Clark CM, Schneider JA, Bedell BJ, et al. Use of florbetapir-PET for imaging beta-amyloid pathology. JAMA 2011;305:275–283.

17. Johnson KA, Sperling RA, Gidicsin CM, et al. Florbetapir (F18-AV-45) PET to assess amyloid burden in Alzheimer's disease dementia, mild cognitive impairment, and normal aging. Alzheimers Dement 2013;9:S72–S83.

18. Klunk WE, Koeppe RA, Price JC, et al. The Centiloid Project: standardizing quantitative amyloid plaque estimation by PET. Alzheimers Dement 2015;11: 115.e11–115.e14.

19. Bittner T, Zetterberg H, Teunissen CE, et al. Technical performance of a novel, fully automated electrochemiluminescence immunoassay for the quantitation of beta-amyloid (1-42) in human cerebrospinal fluid. Alzheimers Dement 2016;12:517–526.

20. Hansson O, Seibyl J, Stomrud E, et al. CSF biomarkers of Alzheimer's disease concord with amyloid-beta PET and predict clinical progression: a study of fully automated immunoassays in BioFINDER and ADNI cohorts. Alzheimers Dement 2018;14: 1470–1481.

21. Korecka M, Waligorska T, Figurski M, et al. Qualification of a surrogate matrix-based absolute quantification method for amyloid-beta(4)(2) in human cerebrospinal fluid using 2D UPLC-tandem mass spectrometry. J Alzheimers Dis 2014;41:441–451.

22. Curtis C, Gamez JE, Singh U, et al. Phase 3 trial of flutemetamol labeled with radioactive fluorine 18 imaging and neuritic plaque density. JAMA Neurol 2015;72: 287–294.

23. Mirra SS, Heyman A, McKeel D, et al. The Consortium to Establish a Registry for Alzheimer's Disease (CERAD), part II: standardization of the neuropathologic assessment of Alzheimer's disease. Neurology 1991;41:479–486.

24. Vemuri P, Whitwell JL, Kantarci K, et al. Antemortem MRI based STructural Abnormality iNDex (STAND)-scores correlate with postmortem Braak neurofibrillary tangle stage. Neuroimage 2008;42:559–567.

25. Palmqvist S, Janelidze S, Stomrud E, et al. Performance of fully automated plasma assays as screening tests for Alzheimer disease-related beta-amyloid status. JAMA Neurol 2019;76:1060–1069.

26. Thal DR, Rub U, Orantes M, Braak H. Phases of A beta-deposition in the human brain and its relevance for the development of AD. Neurology 2002;58:1791–1800.

27. Burnham KP, Anderson DR. Multimodel inference: understanding AIC and BIC in model selection. Sociol Methods Res 2004;33:261–304.

28. Rabinovici GD, Gatsonis C, Apgar C, et al. Association of amyloid positron emission tomography with subsequent change in clinical management among Medicare beneficiaries with mild cognitive impairment or dementia. JAMA 2019;321:1286–1294.

29. Joshi AD, Pontecorvo MJ, Clark CM, et al. Performance characteristics of amyloid PET with florbetapir F 18 in patients with Alzheimer's disease and cognitively normal subjects. J Nucl Med 2012;53:378–384.

30. Clark CM, Pontecorvo MJ, Beach TG, et al. Cerebral PET with florbetapir compared with neuropathology at autopsy for detection of neuritic amyloid-beta plaques: a prospective cohort study. Lancet Neurol 2012;11:669–678.

31. Camus V, Payoux P, Barre L, et al. Using PET with 18F-AV-45 (florbetapir) to quantify brain amyloid load in a clinical environment. Eur J Nucl Med Mol Imaging 2012;39:621–631.

32. Guerra UP, Nobili FM, Padovani A, et al. Recommendations from the Italian Interdisciplinary Working Group (AIMN, AIP, SINDEM) for the utilization of amyloid imaging in clinical practice. Neurol Sci 2015;36:1075–1081.

33. Kobylecki C, Langheinrich T, Hinz R, et al. 18F-florbetapir PET in patients with frontotemporal dementia and Alzheimer disease. J Nucl Med 2015;56:386–391.

34. Perani D, Schillaci O, Padovani A, et al. A survey of FDG- and amyloid-PET imaging in dementia and GRADE analysis. Biomed Res Int 2014;2014:785039.

35. Foster NL, Heidebrink JL, Clark CM, et al. FDG-PET improves accuracy in distinguishing frontotemporal dementia and Alzheimer's disease. Brain 2007;130: 2616–2635.

36. Lin C, Itti E, Haioun C, et al. Early 18F-FDG PET for prediction of prognosis in patients with diffuse large B-cell lymphoma: SUV-based assessment versus visual analysis. J Nucl Med 2007;48:1626–1632.

37. Pontecorvo MJ, Arora AK, Devine M, et al. Quantitation of PET signal as an adjunct to visual interpretation of florbetapir imaging. Eur J Nucl Med Mol Imaging 2017;44: 825–837.

38. Lilja J, Leuzy A, Chiotis K, Savitcheva I, Sorensen J, Nordberg A. Spatial normalization of (18)F-flutemetamol PET images using an adaptive principal-component template. J Nucl Med 2019;60:285–291.

39. Harn NR, Hunt SL, Hill J, Vidoni E, Perry M, Burns JM. Augmenting amyloid PET interpretations with quantitative information improves consistency of early amyloid detection. Clin Nucl Med 2017;42:577–581.

40. McMillan CT, Chetelat G. Amyloid "accumulators": the next generation of candidates for amyloid-targeted clinical trials? Neurology 2018;90:759–760.

41. Mattsson N, Palmqvist S, Stomrud E, Vogel J, Hansson O. Staging beta-amyloid pathology with amyloid positron emission tomography. JAMA Neurol Epub 2019 Jul 17.

42. Thal DR, Beach TG, Zanette M, et al. [(18)F]flutemetamol amyloid positron emission tomography in preclinical and symptomatic Alzheimer's disease: specific detection of advanced phases of amyloid-beta pathology. Alzheimers Dement 2015;11: 975–985.

43. Lundqvist R, Lilja J, Thomas BA, et al. Implementation and validation of an adaptive template registration method for 18F-flutemetamol imaging data. J Nucl Med 2013; 54:1472–1478.

44. Fripp J, Bourgeat P, Raniga P, et al. MR-less high dimensional spatial normalization of 11C PiB PET images on a population of elderly, mild cognitive impaired and Alzheimer disease patients. Med Image Comput Assist Interv 2008;11:442–449.

45. Whittington A, Sharp DJ, Gunn RN, Alzheimer's disease neuroimaging I. Spatiotemporal distribution of beta-amyloid in Alzheimer disease is the result of heterogeneous regional carrying capacities. J Nucl Med 2018;59:822–827.

46. Schneider JA, Aggarwal NT, Barnes L, Boyle P, Bennett DA. The neuropathology of older persons with and without dementia from community versus clinic cohorts. J Alzheimers Dis 2009;18:691–701.

47. Carson RE, Channing MA, Blasberg RG, et al. Comparison of bolus and infusion methods for receptor quantitation: application to [18F]cyclofoxy and positron emission tomography. J Cereb Blood Flow Metab 1993;13:24–42.

48. Salloway S, Gamez JE, Singh U, et al. Performance of [(18)F]flutemetamol amyloid imaging against the neuritic plaque component of CERAD and the current (2012) NIA-AA recommendations for the neuropathologic diagnosis of Alzheimer's disease. Alzheimers Dement (Amst) 2017;9:25–34.

Neurology®

This information is current as of October 19, 2020

Updated Information & Services	including high resolution figures, can be found at: http://n.neurology.org/content/95/21/e2834.full
References	This article cites 47 articles, 13 of which you can access for free at: http://n.neurology.org/content/95/21/e2834.full#ref-list-1
Citations	This article has been cited by 2 HighWire-hosted articles: http://n.neurology.org/content/95/21/e2834.full##otherarticles
Subspecialty Collections	This article, along with others on similar topics, appears in the following collection(s): **Alzheimer's disease** http://n.neurology.org/cgi/collection/alzheimers_disease **PET** http://n.neurology.org/cgi/collection/pet
Permissions & Licensing	Information about reproducing this article in parts (figures,tables) or in its entirety can be found online at: http://www.neurology.org/about/about_the_journal#permissions
Reprints	Information about ordering reprints can be found online: http://n.neurology.org/subscribers/advertise

AMERICAN ACADEMY OF NEUROLOGY®